Probing the light radion through diphotons at the Large Hadron Collider

Satyaki Bhattacharya,[1] Mariana Frank,[2] Katri Huitu,[3] Ushoshi Maitra,[4]
Biswarup Mukhopadhyaya,[4] and Santosh Kumar Rai[4]

[1]*Saha Institute of Nuclear Physics, Sector-I, Block-AF, Bidhannagar, Kolkata 700064, India*
[2]*Department of Physics, Concordia University, 7141 Sherbrooke Street West, Montreal, Quebec, Canada H4B 1R6*
[3]*Department of Physics and Helsinki Institute of Physics, University of Helsinki, P.O. Box 64 (Gustaf Hällströmin katu 2), Helsinki FIN-00014, Finland*
[4]*Regional Centre for Accelerator-Based Particle Physics, Harish-Chandra Research Institute, Chhatnag Road, Jhusi, Allahabad 211019, India*

(Received 12 October 2014; published 26 January 2015)

A radion in a scenario with a warped extra dimension can be lighter than the Higgs boson, even if the Kaluza-Klein excitation modes of the graviton turn out to be in the multi-TeV region. The discovery of such a light radion would be a gateway to new physics. We show how the two-photon mode of decay can enable us to probe a radion in the mass range 60–110 GeV. We take into account the diphoton background, including fragmentation effects, and include cuts designed to suppress the background to the maximum possible extent. Our conclusion is that, with an integrated luminosity of 3000 fb^{-1} or less, the next run of the Large Hadron Collider should be able to detect a radion in this mass range, with a significance of 5 standard deviations or more.

DOI: 10.1103/PhysRevD.91.016008 PACS numbers: 11.10.Kk, 12.60.-i, 14.80.-j

I. INTRODUCTION

The Large Hadron Collider (LHC) data from the $\sqrt{s} = 7$ and 8 TeV runs analyzed by the ATLAS [1] and CMS [2] Collaborations have more or less confirmed a scalar particle whose properties agree with those of the Standard Model (SM) Higgs boson. Although more analyses are needed to confirm it to be purely the SM Higgs with exact SM-like couplings, the question as to whether the SM is the final theory is still very much open.

Issues ranging from the naturalness of the Higgs mass to the dark matter content of the Universe suggest physics beyond the standard model (BSM). This has prompted physicists to look for new particles or symmetries around the TeV scale. The lack of new physics signals at the LHC may carry the message that we have to seek somewhat higher scales to see BSM physics, especially if it exists in one of the currently popular forms. That, in turn, has led to conjectures about new physics above 1 TeV, which can still address the naturalness issue, albeit with some degree of fine-tuning. In the process, however, a question that is perhaps not being asked with sufficient emphasis is, could new physics, for a change, lie hidden at a relatively low mass scale, not yet discovered just because of experimental difficulties in unraveling it? We address one such instance in this paper.

In this context, one BSM scenario which catches one's imagination is one with a warped extra spacelike dimension, first proposed by Randall and Sundrum (RS). The RS model provides an elegant explanation of the large hierarchy between the electroweak scale (100 GeV to 1 TeV) and the Planck scale (10^{19} GeV) in terms of an exponential damping of the gravitational field across a small compact fifth dimension, without invoking unnaturally large numbers [3]. This is achieved through a nonfactorizable geometry with an exponential warp factor, whereas the additional spatial dimension is compactified on a S_1/Z_2 topology which corresponds to a once-folded circle, with two D_3-branes sitting at the orbifold fixed points. The original RS model is based on the assumption that the S M fields are localized on one of the D_3-branes (called the visible brane, at $y = r_c\pi$, where r_c is the radius of the compact dimension and y is the coordinate along that dimension) and only gravity propagates in the bulk. Compactification results in a massless state and a tower of massive modes of the spin-2 graviton on the visible brane. While resonant production and decays of the massive graviton are rather spectacular phenomena, the absence of such signals has pushed the lower limit on the massive modes to about 2.7 TeV [4].

The radius of the extra dimension in the RS model is assumed to be fixed by a given constant and needs stabilizing against quantum fluctuations parametrized by a scalar field ($\varphi(x)$), viz. the radion. Goldberger and Wise [5] proposed a mechanism for radius stabilization by showing that a bulk scalar field propagating in the warped geometry can generate a potential for this radion field and in the same process, dynamically generate a vacuum expectation value (VEV) for $\varphi(x)$ required to stabilize the radius to the constant value needed to address the hierarchy of the electroweak scale and the Planck scale. Its mass, however, can be much lighter than those of the massive gravitons [6]. The radion coupling to SM fields is governed by its VEV, $\Lambda_\varphi(\simeq\text{TeV})$ and the trace of the energy-momentum tensor (T^μ_μ) [7]. At LEP, such a light radion could have been produced via $e^+e^- \to Z\varphi$. The production mode in this channel is however found to be suppressed for $\Lambda_\varphi > 1.0$ TeV and hence, a radion as light as 50–100 GeV with $\Lambda_\varphi \simeq 2$–3 TeV is still allowed by LEP data as well as by LHC searches [8–10]. The radion can in principle mix with the Higgs boson through terms consistent with general covariance. The phenomenology of such a mixed state has been considered in detail in the literature [11–20] and more recently has been reinvestigated [21–27] in light of the discovery of the ∼125 GeV scalar resonance at LHC. Similarly, the phenomenology of the simpler scenario of an unmixed radion, too, has been studied quite thoroughly [28–34]. In this work we restrict ourselves to the unmixed scenario such that the scalar resonance observed at LHC is a pure SM Higgs boson (h). We concentrate on identifying the most promising signals for an unmixed light radion ($m_\varphi < m_h$), which could provide the first observable signals for models of extra spatial dimensions with warped geometry. Our results can be very easily generalized to the mixed scenario as well, and are also applicable to extensions of the RS model where the SM fields propagate in the bulk. We focus primarily on the following interesting highlights of a light radion signal at the LHC:

(i) An unmixed radion lighter than the 125 GeV Higgs can have an appreciable production cross section for allowed values of the VEV (2 TeV $< \Lambda_\varphi <$ 3 TeV), primarily through gluon fusion. A factor that contributes to this, namely, the trace anomaly contribution, boosts the loop induced decay modes of the radion into a pair of massless gauge bosons. This can partially compensate for the Λ_φ suppressions in its couplings to SM particles.

(ii) A light radion with mass below 100 GeV is not ruled out by any experiments [35]. We show that the channel ($\gamma\gamma$) which helped discover the SM Higgs with the maximum significance would also be the most promising channel for such a light radion at the LHC.

(iii) The radion loop-induced decay mode ($\gamma\gamma$) also acquires an enhancement from the trace anomaly (which interferes constructively with the dominant W boson mediated loop amplitude) and yields a reasonably healthy, *albeit* small diphoton branching rate for radion masses below 120 GeV.

One must note that the radion signal depends crucially on the value of Λ_φ which suppresses the effective coupling of the radion to SM fields as the couplings are inversely proportional to the value of Λ_φ. Current constraints on the KK excitations of the spin-2 graviton already put a lower bound on the value of the Λ_φ [4].

For a radion of mass $\simeq$100 GeV and lower, the dominant decay modes are gluon-gluon and $b\bar{b}$, while the branching ratios into WW^*/ZZ^* are suppressed. The signal arising from $b\bar{b}$ and gg are beset with large QCD backgrounds, even if we consider various associated production channels. Thus, with the enhanced gg fusion as the production mode, $\varphi \to \gamma\gamma$ becomes the best channel for observing the light radion at the LHC. Since a peak in the diphoton invariant mass is a rather spectacular signal of new physics, the refinement of techniques to isolate two photons can be helpful in a more general context as well.

With the impressive performance of the electromagnetic calorimeter at the CMS and ATLAS experiments, and optimized event selection criteria for the diphoton signal, we have been able to observe the SM Higgs boson with large significance, even with nominal luminosities available at the 7 and 8 TeV runs. We are about to enter a regime of higher intensity running of the LHC with roughly double the center of mass energies. In view of this, the prospects of observing a light radion in the same mode are good. We demonstrate this with a detailed analysis of the radion signal and the SM background in the $pp \to \gamma\gamma + X$ events at the 14 TeV run of LHC.

The SM backgrounds for these events are of course formidable. As for the case of Higgs signals, the $\gamma\gamma$ final state has backgrounds from not only prompt photon pairs, but also γj and jj production. Of these, the γj background can be substantial, especially for low diphoton invariant mass. We followed the cuts commonly used by ATLAS and CMS for reducing these backgrounds without compromising too much on the signal rates [10,36].

Our paper is organized as follows. In Sec. II we describe briefly the RS model with an unmixed radion. In Sec. III we present our analysis and results for observing the radion in the diphoton channel. We finally summarize and conclude in Sec. IV. Additional formulas for production and decay of the radion are provided in the appendixes.

II. THE RADION IN MODELS WITH A WARPED EXTRA DIMENSION

In the original version of the Randall-Sundrum model, there is an extra spacelike dimension, namely, $y = r_c\phi$, which is S^1/Z_2 orbifolded. Two 3-branes with tensions of opposite signs are present at the orbifold fixed points $\phi = 0$ and $\phi = \pi$. Gravity propagates in the bulk and it mainly peaks at the first brane ($\phi = 0$), called the hidden brane, whereas all other SM fields propagate on the second brane ($\phi = \pi$), called the visible brane. The resulting nonfactorizable 5-dimensional metric depends on the radius of compactification (r_c) of the additional dimension

$$ds^2 = e^{-2kr_c\phi}\eta_{\mu\nu}dx^\mu dx^\nu + r_c^2 d\phi^2. \tag{1}$$

The Planck mass associated with the 4-dimensional space-time ($M_{\rm Pl}$) is of the same order of magnitude as the 5-dimensional space-time Planck mass (M). They are related by

$$M_{\rm Pl}^2 = \frac{M^3}{k}(1 - e^{-2kr_c\phi}). \tag{2}$$

A field that propagates on the visible brane in the 5-dimensional theory carrying a mass parameter m_0 generates a physical mass $m = m_0 e^{-k\pi r_c}$ in the 4-dimensional effective theory. For the value of $kr_c \simeq 12$, the Planck scale is reduced to the weak scale, thus solving the hierarchy problem.

The above metric allows two types of massless excitation. The first one is the fluctuation of the flat background metric that generates a bulk graviton. The second conceivable fluctuation is that of the compactification radius r_c, which can be expressed as $T(x)$, where T is a modulus field.

The Kaluza-Klein (KK) decomposition of the bulk graviton on the visible brane generates a discrete tower of states, with the zero mode as the massless graviton mode. The mass of the nth KK mode of the graviton is given by

$$m_n = kx_n e^{-kr_c\pi}, \tag{3}$$

where x_n is the nth root of J_1, the Bessel function of order 1.

The massless mode of the graviton couples to matter with a strength suppressed by the Planck mass. The corresponding couplings of the massive KK modes are suppressed at the TeV scale, with an effective coupling given by $k/\bar{M}_{\rm Pl}$, where $\bar{M}_{\rm Pl}$ is the reduced Planck mass. The KK excitations of the graviton can be directly probed at the LHC and recent experimental limits from available LHC data rule out the possibility of a mass below 2.67 TeV for the first KK mode graviton with $k/\bar{M}_{\rm Pl} = 0.1$ [4].

However, there is one more new physics component of the RS scenario. The radius r_c of the compact dimension seems to be frozen *ad hoc* at the requisite value for solving the hierarchy problem. This arbitrariness is removed if, as stated earlier, r_c can be construed as the VEV of a modulus field $T(x)$ which quantifies the fluctuation about the stabilized radius. With this, the metric becomes

$$ds^2 = e^{-2kT(x)\varphi} g_{\mu\nu}(x) dx^\mu dx^\nu + T^2(x) d^2\varphi. \tag{4}$$

After Kaluza-Klein reduction of the 5-dimensional action and after integrating out the additional coordinate, the $T(x)$ dependent part of the action is

$$S = 2\frac{M^3}{k}\int d^4x\sqrt{-g(x)}R(1 - e^{-2kT(x)\pi}) + \frac{3M^3}{k}\int d^4x\sqrt{-g(x)}\partial_\mu(e^{-k\pi T(x)})\partial^\mu(e^{-k\pi T(x)}). \tag{5}$$

Defining $\varphi(x) = \Lambda_\varphi e^{-k[T(x)-r_c]\pi}$ with $\Lambda_\varphi = \sqrt{\frac{6M^3}{k}}e^{-kr_c\pi}$, Eq. (5) becomes

$$S = \frac{2M^3}{k}\int d^4x\sqrt{-g}\left(1 - \left(\frac{\varphi}{f}\right)^2\right)R + \frac{1}{2}\int d^4x\sqrt{-g}\partial_\mu\varphi\partial^\mu\varphi. \tag{6}$$

This $\varphi(x)$ field is known as the radion field. However, at this point there is no mechanism of stabilizing the radion field such that $T(x)$ acquires its desired VEV r_c, since φ is *prima facie* massless. This stabilization is implemented through the Goldberger-Wise mechanism where an additional bulk scalar field is introduced, which develops an effective 4-dimensional potential on the brane. This potential generates the mass as well as the VEV of the radion. The parameters of the potential have to be such that it attains its minima for $kr_c = 12$. The mass of the radion, essentially a free parameter, can be smaller than the TeV scale, even when the massive graviton modes are much heavier. The principle of general covariance allows the radion to couple with matter through the trace of the energy-momentum tensor. Its interaction with the SM particles is given by

$$\mathcal{L}_{\rm int} = T^\mu_\mu \frac{\varphi}{\Lambda_\varphi}, \tag{7}$$

where T^μ_μ is the trace of energy momentum tensor $T_{\mu\nu}$. Thus, the interaction of the radion with the massive SM particles is given by

$$\mathcal{L}_1 = \frac{\varphi}{\Lambda_\varphi}\left(\sum_f m_f f\bar{f} - 2m_W^2 W_\mu^+ W^{\mu-} - m_Z^2 Z_\mu Z^\mu + (2m_h h^2 - \partial_\mu h \partial^\mu h)\right). \tag{8}$$

The mass (m_φ) and VEV (Λ_φ) of the radion determine its phenomenology, similarly to the case of the SM Higgs. The mass of the first KK mode of graviton m_1, $k/\bar{M}_{\rm Pl}$ and the Λ_φ are related by

$$\frac{k}{\bar{M}_{\rm Pl}} = \frac{\sqrt{6}m_1}{\Lambda_\varphi x_1} \quad \text{with} \quad x_1 = 3.83. \tag{9}$$

To suppress higher curvature terms, $\frac{k}{\bar{M}_{\rm Pl}}$ should not be greater than 1. Thus, the absence of the first KK mode of graviton at the LHC till 2.67 TeV implies a lower limit of about 1.8 TeV on the radion VEV [4,35,37].

The effective couplings of φ with gluon and photon pairs are slightly different and have two components. The first one, just like for the SM Higgs, comes from the amplitude of the one-loop diagrams dominantly involving the top quark, and the W boson for the photon. The second contribution arises from the trace anomaly for the massless gauge field. Thus, the interaction of the radion with a gluon pair is given by

$$\mathcal{L}_2 = \frac{\alpha_s}{16\pi} G_{\mu\nu} G^{\mu\nu} [2b_3 - F_{1/2}(\tau_t)] \frac{\varphi}{\Lambda_\varphi}, \quad (10)$$

where $b_3 = 7$ is the QCD β function. The effective diphoton interaction of the radion is similarly given by

$$\mathcal{L}_3 = \frac{\alpha_{\mathrm{EM}}}{8\pi} F_{\mu\nu} F^{\mu\nu} \left[(b_2 + b_Y) - \left(F_1(\tau_W) + \frac{4}{3} F_{1/2}(\tau_t) \right) \right] \frac{\varphi}{\Lambda_\varphi}, \quad (11)$$

where $b_2 = 19/6$ and $b_Y = -41/6$ are the SM $SU(2)$ and $U(1)_Y$ β functions respectively.

In principle, the radion can mix with the SM Higgs via general covariant terms, which trigger a kinetic mixing. The coefficient of this mixing term can affect the phenomenologies of both the radion and the Higgs field. As has been stated in the Introduction, our purpose here is to find out signals of a light radion, for which such mixing is neglected in the first approximation.

III. ANALYSIS OF THE RADION IN THE TWO-PHOTON CHANNEL

A. Radion production and decay at the LHC

At hadron colliders, the radion can be produced via gluon fusion or through W or Z fusion, and can also have associated production modes with W, Z bosons and $t\bar{t}$. The first of the aforementioned production modes receives a sizable boost from trace anomaly. The radion can also be produced in association with a W or Z boson. The radion produced in association with a gauge boson can decay to $b\bar{b}$ with sizable cross section. The final state will be either dilepton plus two b-jets or single lepton plus two b-jets. But the associated production channel is not of much use, due to its suppression by Λ_φ, in contrast to the gluon-fusion channel where the trace anomaly term at least partially compensates with an enhancement. We analyzed the final states for such a signal and found that the SM dilepton background and single lepton background overwhelm the signal and are roughly 3 to 4 orders of magnitude higher than the signal. Another possibility is the production of the radion via vector boson fusion and its subsequent decay to $b\bar{b}$. Here too, the suppression in couplings by the radion VEV is a problem; and on the whole, the $2j + b\bar{b}$ SM background is also found to be larger than the signal by 4 to 5 orders of magnitude [38]. The most promising production channel thus remains the gluon fusion.

The production cross section of the radion in gluon fusion channel at the LHC is illustrated in Fig. 1(a) for 13 and 14 TeV center of mass energies. Since the cross sections are of comparable magnitudes, we present the rest of our results for 14 TeV, with the understanding that the predictions are generally valid if a part of the LHC run is at 13 TeV center of mass energy.

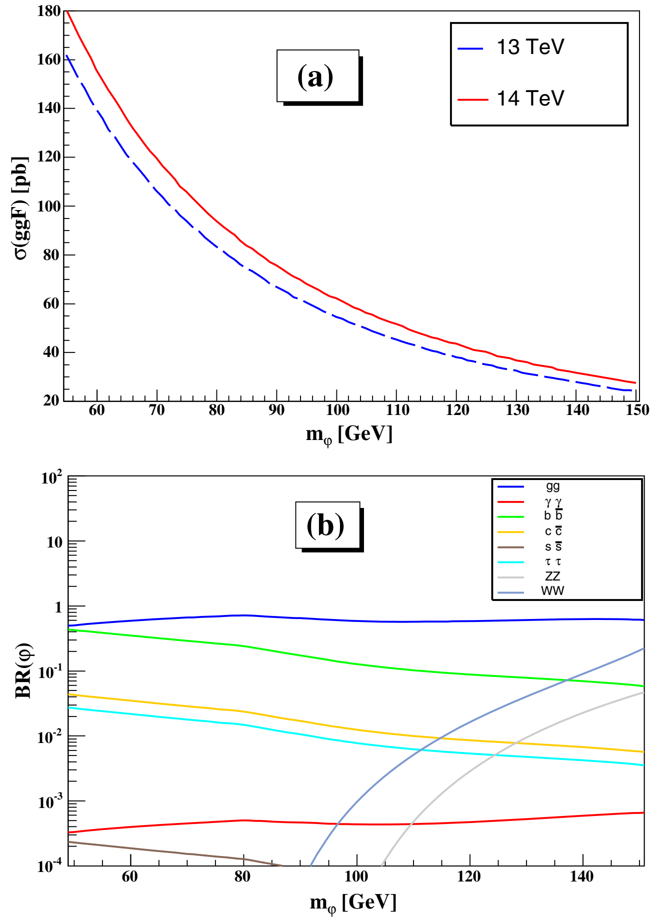

FIG. 1 (color online). (a) Production cross section of radion via gluon fusion versus m_φ for 13 and 14 TeV center of mass energies at the LHC. (b) Branching ratios for the radion decay modes as functions of its mass m_φ.

We used a radion VEV, $\Lambda_\varphi = 2$ TeV in most of our subsequent analysis. The cross section corresponding to any other Λ_φ can be obtained by simple scaling. The branching ratios of the radion to all possible final states are shown in Fig. 1(b). Note that the different branching ratios of the radion decay are independent of Λ_φ, since all interactions of the radion with SM particles are inversely proportional to it, including the radion width.

As seen from Fig. 1(b), when the mass of the radion is less than 100 GeV, it decays dominantly into two gluons. However the two gluon final state gets swamped by the large QCD background at the LHC, making it a very difficult channel to observe any signal for a light radion.

This leaves two potential channels in which a light radion can be probed, namely, $\gamma\gamma$ and $\tau^+\tau^-$. From the experience with the Higgs boson, various subtleties involved in the analysis of a $\tau^+\tau^-$ final state make it more suitable as a channel which will confirm the presence of the radion, rather than one used for discovery. Furthermore, a light radion produces relatively softer τ's, which can stand in the way of efficient identification. The diphoton final state, on the other hand, is more spectacular in terms of reconstruction, in spite of the low branching ratio. Thus the diphoton channel, when it comes to uncovering a radion in the mass range 60–110 GeV, remains the most promising, and we analyze it next.

B. The diphoton channel: Signal and backgrounds

As stated, the diphoton channel for the radion is one with very high sensitivity, and should be given priority in the explorations at the 14 TeV run of the LHC. In our study we have varied the mass of the radion from 60 to 110 GeV. The status of a heavier radion can be surmised from the 8 TeV run itself, for example, from Refs. [21,28] in the zero-mixing limit. The diphoton signal for a radion of mass $m_\varphi > 100$ GeV has also been considered in [39]. However, that analysis is based on a model with gauge fields in the bulk, where the diphoton rate receives an enhancement.[1] Our study addresses a situation where (a) such enhancement is absent and (b) the radion is lighter than 100 GeV. On both counts, overcoming the backgrounds thus becomes a tougher challenge for us.

Two isolated photons in the final state can be mimicked by many SM processes. We classify the processes into two categories, reducible and irreducible.

(i) The irreducible background consists of two prompt photons in the final state. It originates from the tree level production via $q\bar{q}$ annihilation (Born process) as well as from the one-loop process (box diagram) in gluon fusion with quarks running in the loop. The contribution from the latter is comparable to that from the Born level process because of the high gluon flux at low x, where x represents the energy fraction of the colliding proton energy carried by the partons. These photons are as isolated as those arising from radion decay. Such isolated photon pairs constitute an irreducible background to the signal in any search window for a mass peak [40].

(ii) The dominant reducible background arises from a prompt photon along with a jet. A π^0, a ρ or an η decays into two collimated photons that are identified as a single electromagnetic cluster in the detector. This causes the misidentification of jets as hard isolated photons. Although the probability of this misidentification in a particular event is small, the sheer volume of the γj cross section turns it into a serious background. We suggest ways of reducing this kind of background in the subsequent analysis.

(iii) Similarly, as above, two jets can be misidentified as a pair of isolated photons. The double misidentification probability, however, is small, and the dijet background is not significant in the present analysis.

(iv) The Drell-Yan production of e^+e^- can also mimic diphotons, if the $e^\pm$ tracks are not correctly reconstructed by the inner tracking chamber. We convolute the Drell-Yan background with a typical inefficiency of 5% for the track detector at the LHC [41].

C. Signal versus background: The phoenix effect

The signal events are generated in MADGRAPH 5 [42], where the interaction vertices of the radion are included using the FEYNRULES [43] package. We have used PYTHIA 8 [44] for showering and hadronization of the signal events as well as for generating background events. We adopted CTEQ6l1 [45] as our parton density function (PDF). The renormalization and factorization scales are kept at the default value of PYTHIA 8. To obtain sufficient statistics for the signal as well as for the background events, we divided our whole analysis into different phase space regions distinguished by the value of the radion mass. For this purpose, we designated different regions of $\hat{\mathrm{m}}$ (the invariant mass of the outgoing partons), for different mass values of the radion:

(i) For $\mathrm{m}_\varphi = 60$ GeV: 45 GeV $\leq \hat{\mathrm{m}} \leq$ 75 GeV;
(ii) For $\mathrm{m}_\varphi = 70$ GeV: 55 GeV $\leq \hat{\mathrm{m}} \leq$ 85 GeV;
(iii) For $\mathrm{m}_\varphi = 80$ GeV: 65 GeV $\leq \hat{\mathrm{m}} \leq$ 95 GeV;
(iv) For $\mathrm{m}_\varphi = 90$ GeV: 75 GeV $\leq \hat{\mathrm{m}} \leq$ 105 GeV;
(v) For $\mathrm{m}_\varphi = 100$ GeV: 85 GeV $\leq \hat{\mathrm{m}} \leq$ 115 GeV;
(vi) For $\mathrm{m}_\varphi = 110$ GeV: 95 GeV $\leq \hat{\mathrm{m}} \leq$ 125 GeV.

For realistic background estimations, we implemented an algorithm at the generator level, which approximates the clustering procedure in a typical electromagnetic calorimeter (ECAL). Specifically, we used the dimension of an ECAL crystal of the Compact Muon Solenoid (CMS) detector. The ECAL at the CMS is made up of lead tungstate ($PbWO_4$) crystals. A single crystal of the ECAL covers 0.0175×0.0175 in the $\eta - \phi$ plane. The electromagnetic shower from an unconverted photon is contained within a 5×5 crystal matrix around the seed crystal (i.e., the one hit by the photon). In case of a converted photon, the typical region of energy deposit is wider. In order to make the analysis robust, we used a 10×10 crystal size for photon reconstruction, equal to $\triangle\mathrm{R} = 0.09$ (where $\triangle\mathrm{R} = \sqrt{\triangle\eta^2 + \triangle\phi^2}$) in the $\eta - \phi$ plane of the CMS detector. The momentum of the photon candidate is defined as the vector sum of the photon and electron momenta falling within the cone $\triangle\mathrm{R} = 0.09$ around the seed, which is either a direct photon or an electron.

To account for finite detector resolutions, we smeared the photon, electron and jet energies with Gaussian functions [46]. We selected the photon seeds satisfying $|\eta| < 3.0$. The reconstructed photon candidates are then accepted if they satisfy the preselection criteria given as

(i) $\mathrm{p}_\mathrm{T}^{\gamma,\mathrm{leading}} > 15$ GeV and $\mathrm{p}_\mathrm{T}^{\gamma,\mathrm{subleading}} > 10$ GeV;
(ii) $|\eta_\gamma| < 2.5$.

[1]Other mechanisms leading to enhancement in the diphoton channel also exist [33].

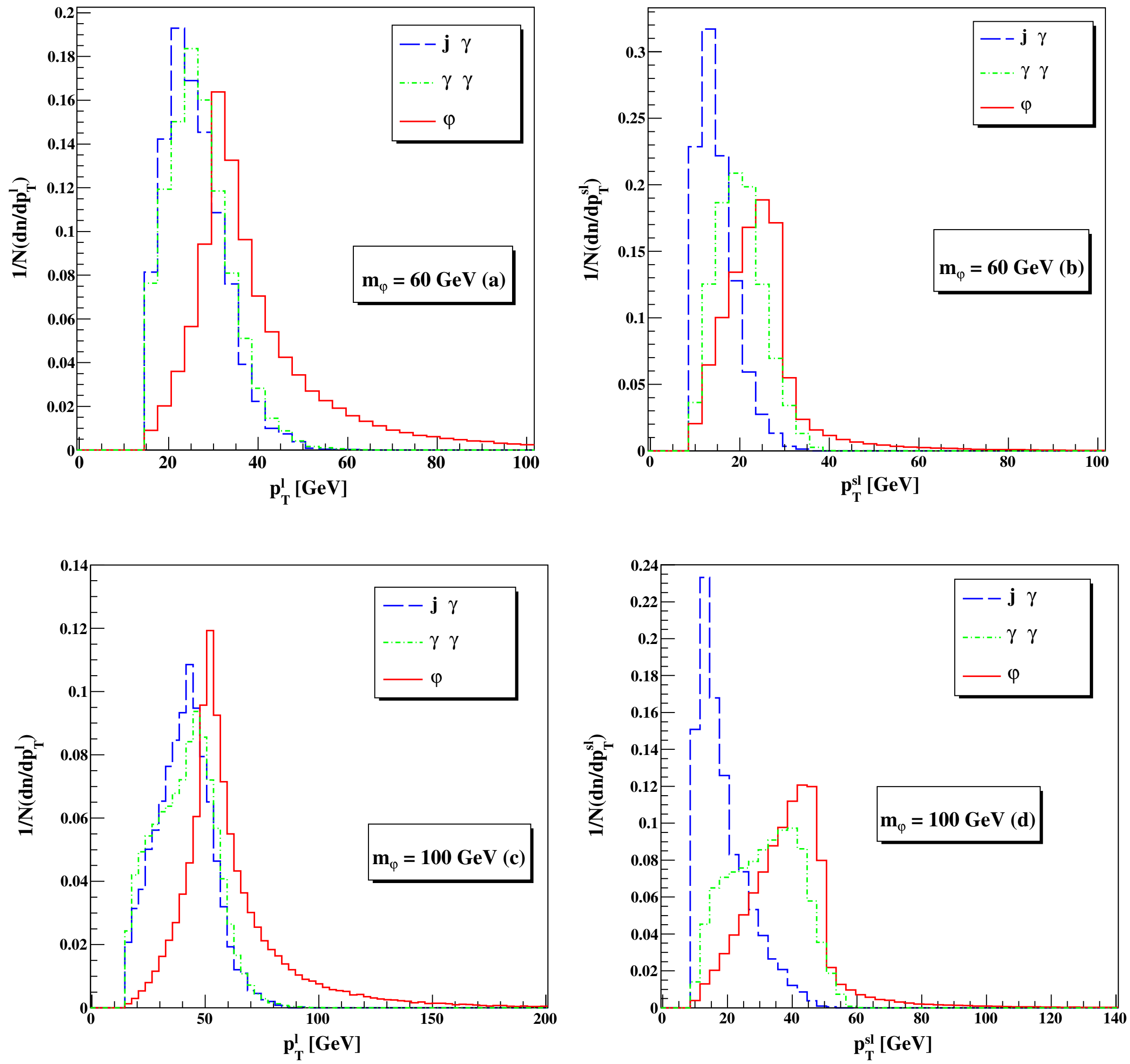

FIG. 2 (color online). Normalized distribution of p_T^γ for two sample masses of radion, diphoton background and signal photon background. (a) Normalized distribution of $p_T^{\gamma,\mathrm{leading}}$ for $m_\varphi = 60$ GeV; (b) Normalized distribution of $p_T^{\gamma,\mathrm{subleading}}$ for $m_\varphi = 60$ GeV; (c) Normalized distribution of $p_T^{\gamma,\mathrm{leading}}$ for $m_\varphi = 100$ GeV; (d) Normalized distribution of $p_T^{\gamma,\mathrm{subleading}}$ for $m_\varphi = 100$ GeV.

The $|\eta|$-interval is reduced further to emulate the inefficient tracker region. These triggered photon candidates are required to have minimal hadronic activity. Jets are reconstructed in our analysis with $|\eta| < 4.5$ and $p_T^j > 10$ GeV using an anti-k_t algorithm [47]. Photons arising from the jets are rejected by demanding that the scalar sum of the entire transverse energy within a cone of $\triangle R = 0.4$ be less than 4 GeV.[2] Only those isolated photons which survive the above selection criteria qualify for our final analysis.

[2]This is an "absolute isolation" criteria. One can alternatively require a relative isolation, demanding that the total visible p_T within $\Delta R = 0.4$ be less than 10% from that of the photon. This raises the statistical significance for a lower mass of m_φ.

The p_T^γ distributions for background and signal are plotted in Figs. 2(a), 2(b) for $m_\varphi = 60$ GeV, and in Fig. 2(c), 2(d) for $m_\varphi = 100$ GeV. Other kinematic variables, such as angular separations, can be used as good discriminators at the generator level. However, once the detector resolutions are taken into account the distinct features of these variables are smeared. We find that the background coming from a prompt photon and a jet dominates over the two prompt photon backgrounds in the low ($p_T^\gamma < 35$ GeV) region. With increasing p_T^γ, the jet-γ misidentification rate decreases and hence the γj background falls gradually. Though the Drell-Yan background is 2 orders of magnitude lower than the direct photon background, it increases near the Z mass pole, and is comparable to the direct photon backgrounds. We find that the two-jet background is negligible, and thus we do not consider it in our analysis. As seen in Fig. 2, radion mass-specific $\mathrm{p}_\mathrm{T}^{\gamma}$-cuts are effective, in view of the fact that a heavier radion generally yields harder photons. For a heavier radion, the fraction of events with harder $\mathrm{p}_\mathrm{T}^{\gamma}$ in the signal is large compared to the background. Thus, it is easier to separate the signal events from the background by selecting harder photon candidates. The mass dependent p_T-cuts in our analysis are formulated as

$$\mathrm{p}_{\mathrm{T}\times\mathrm{min}}^{\mathrm{leading}} = (m_\varphi/2\text{–}5.0)\ \mathrm{GeV};$$
$$\mathrm{p}_{\mathrm{T}\times\ \mathrm{min}}^{\mathrm{subleading}} = (\mathrm{p}_{\mathrm{T}\times\mathrm{min}}^{\mathrm{leading}} - 5.0)\ \mathrm{GeV}. \tag{12}$$

We finally select only those events that fall within the invariant mass window of ± 3.5 GeV about the radion mass. If we consider the invariant mass window to be about 5 GeV, the background rate increases, thus reducing the signal-to-background significance $(S/\sqrt{B})$.

The cut flow for the signal with 60 and 90 GeV radion mass and the corresponding SM background are presented in Table I. The mass dependent cuts along with the final signal-to-background significance are shown in Table II. In Fig. 3(a), we plot the integrated luminosity required to achieve 5σ significance level for different radion masses. In Fig. 3(b), we also plot the maximum VEV of the radion that can be probed with 5σ significance level for different mass values of the radion with two choices of the integrated luminosity. Note that these results do not conflict with the recent ATLAS search [10] at $\sqrt{s} = 8$ TeV and with luminosity $\mathcal{L} = 20.3\ \mathrm{fb}^{-1}$. The data rule out signals with $\sigma_{gg} \times \mathrm{BR}(\varphi \to \gamma\gamma)$ of 30 fb or more, while the signal rate for $\sqrt{s} = 8$ TeV in our scenario is smaller in magnitude.

Figure 4 shows the invariant mass peak of the signal against the background, for $m_\varphi = 60$ GeV. For an efficient modeling of the background, a low-luminosity histogram for the background has been generated first. Thereafter, a fitting function has been used to improve it, thus yielding the background for a luminosity of $3000\ \mathrm{fb}^{-1}$. It should also be noted that the bump corresponding to the signal is sitting on the edge of the rising part of the background. This is in contrast with the familiar figure for Higgs reconstruction, where the bump is seen against a monotonically falling background profile. This effect is due to the strong p_T-cuts that we must impose on the

TABLE I. Cut flow table for two different values of radion mass, $m_\varphi = 60$ GeV and $m_\varphi = 90$ GeV.

m_φ		$\varphi \to \gamma\gamma$	$\gamma\gamma$	$j\gamma$	e^+e^-	$b_1 + b_2 + b_3$
(GeV)	Cuts applied	S (fb)	b_1 (pb)	b_2 (pb)	b_3 (pb)	B (pb)
	Initial signal	39.88	226.84	218109.90	133.78	218470.52
	Preselection	30.80	87.88	6332.58	0.67	6421.13
60	Isolation	24.51	76.76	973.20	0.55	1050.51
	$\mathrm{p}^{\gamma,l} > 27$ GeV					
	$\mathrm{p}_T^{\gamma,sl} > 22$ GeV	14.02	19.15	49.73	0.22	69.10
	$56.5 < \mathrm{m}_{\gamma\gamma} < 63.5$ (GeV)	13.98	6.35	22.68	0.05	29.08
	Initial signal	30.84	48.28	46788.40	1598.90	48435.58
	Preselection	25.00	18.20	3198.46	10.60	3227.26
90	Isolation	19.50	15.59	309.65	8.48	333.72
	$\mathrm{p}^{\gamma,l} > 40$ GeV					
	$\mathrm{p}^{\gamma,sl} > 35$ GeV	9.59	3.77	7.29	3.72	14.78
	$86.5 < \mathrm{m}_{\gamma\gamma} < 93.5$ (GeV)	9.58	1.04	2.15	2.44	5.63

TABLE II. Selection cut, background reduction and significance at 14 TeV cm energy and $3000\ \mathrm{fb}^{-1}$ integrated luminosity for different values of radion mass, m_φ. The signal-to-background significance, σ, is defined by $S/\sqrt{B}$.

m_φ	$p_T^{\gamma,\mathrm{leading}}, p_T^{\gamma,\mathrm{subleading}}$	$m_{\gamma\gamma}^{\mathrm{min}}, m_{\gamma\gamma}^{\mathrm{max}}$	S	B	σ
(GeV)	(GeV)	(GeV)	(fb)	(pb)	$S/\sqrt{B}$
60	27.0, 22.0	56.5, 63.5	13.98	29.07	4.49
70	30.0, 25.0	66.5, 73.5	13.78	15.50	6.06
80	35.0, 30.0	76.5, 83.5	11.42	8.31	6.86
90	40.0, 35.0	86.5, 93.5	9.58	5.63	6.99
100	45.0, 40.0	96.5, 103.5	8.21	1.80	10.60
110	50.0, 45.0	106.5, 113.5	7.04	0.79	13.72

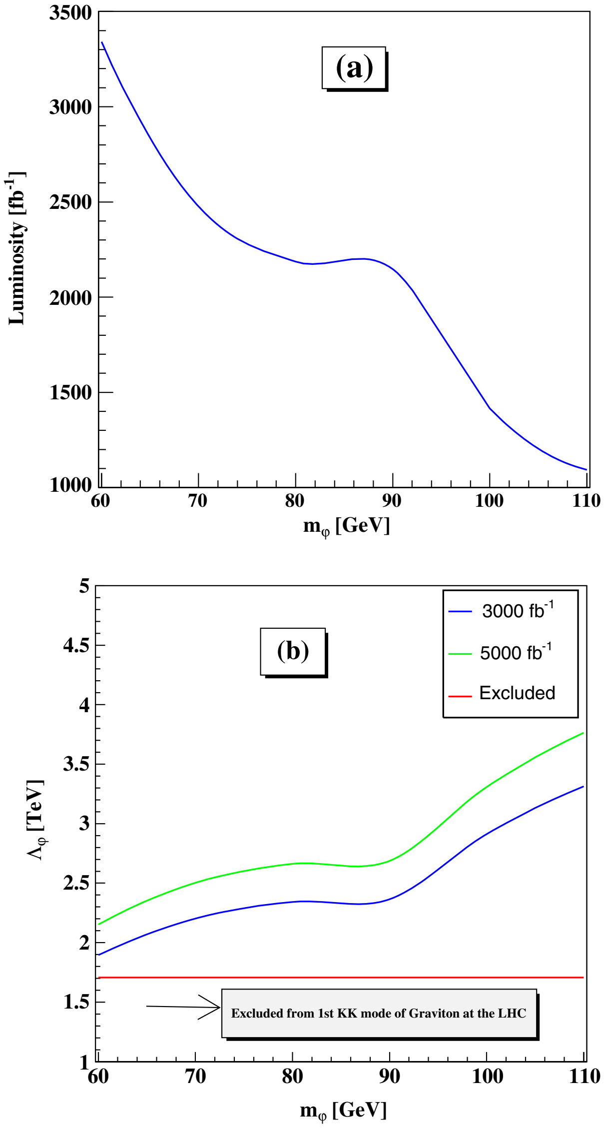

FIG. 3 (color online). (a) Luminosity required for 5σ discovery of radion with m_φ with $\Lambda_\varphi = 2$ TeV. (b) Maximum Λ_φ for a radion to be discovered at 5σ with m_φ.

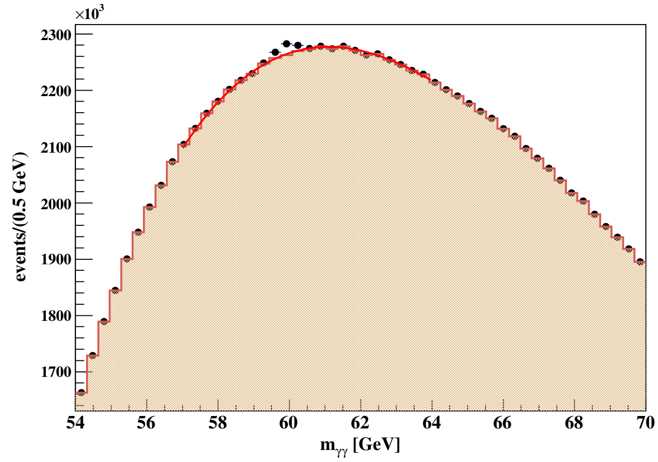

FIG. 4 (color online). Invariant mass peak of the signal against the background, for $m_\varphi = 60$ GeV.

photons, causing an additional background suppression for low $m_{\gamma\gamma}$.[3]

At this point, we should emphasize that we have carried out our analysis at the leading order (LO). To estimate how the predictions differ when including next-to-leading order (NLO) effects, one notices that the K-factor for the production of an 80 GeV Higgs is approximately 2.0 [48]. For diphotons (including the fragmentation contribution), the same K-factor is around 1.3 [40,49]. Therefore, the inclusion of the NLO effects will, if anything, enhance our predicted significance. We also estimated the effects of varying the renormalization and factorization scales, which are set to be equal. The results presented here are based on using the default value for the renormalization scale (Q^2) of the event generator. Changing the scale to $Q^2 = {m_{\gamma\gamma}}^2$ and calculating the uncertainty by varying the scale from $Q^2/2$ to $2Q^2$, the signal and the background event rates change by about $\pm 10\%$.

To report the significance of a diphoton mass peak we have used a simple $S/\sqrt{(B)}$ statistic. An alternative analysis using a likelihood ratio is also possible [36,50,51]. While our cut-based analysis is illustrative in nature, there is scope for improving the sensitivity of this channel by using more sophisticated techniques. If for example, one uses multivariate techniques, then the signal significance improves by a factor of 2. Furthermore, on splitting the sample in several categories of different purities, one expects an enhancement of about 1.5 times in signal significance.

IV. SUMMARY AND CONCLUSIONS

While graviton excitations are immediately recognizable signals of warped extra dimensions, spectacular as such signals can be, the limit on the mass of the lowest such excitation is increasing rather rapidly. In view of this it is important to realize that the radion, connected in a compelling way to the stabilization of the extra dimension(s), can still be quite light, consistently with data available so far.

In this work, we indicated a method for detecting the signature of a light radion, in the range 60–110 GeV, at the LHC. After analyzing all production and decay mechanisms, the diphoton decay channel following gluon fusion production emerges as the best and most promising signal. We thus focused on a pair of photons reconstructed to a peak at various mass windows, and applied cuts that can

[3]It should be noted that we have assumed perfect identification of the vertex from where the photon is coming. In reality, due to presence of pileup vertices, photon vertex identification has a finite efficiency, which can degrade the mass resolution, and consequently the significance.

potentially suppress the backgrounds, where the prompt $\gamma\gamma$ production (at both the Born and box diagram levels) constitute the irreducible SM backgrounds. Event selection criteria have been suggested to reduce this as well as the (dominant) γj background, where the latter is responsible for producing a fake photon. After carrying out a detailed study using parametrized simulation and taking into account all backgrounds, we find that one can separate the signal with a significance of 5σ or more, for an integrated luminosity of up to 3000 fb^{-1}. In general, less luminosity is required for a higher radion mass, as the background falls rapidly with increasing diphoton invariant mass. The diphoton mode also avoids any problem near the Z-pole, except of course the possibility of fakes from electron-positron pairs, which is found to be small.

Notwithstanding the fact that the original RS model has gone through several extensions where SM fields have been allowed to move in the bulk, radion phenomenology has not become markedly different in such extended versions. Thus our results are valid even in extensions of the RS model that allow SM fields in the bulk. Moreover, we have studied here the case of the unmixed radion. If the radion and the Higgs boson are allowed to mix, under certain circumstances this mixing could enhance the mixed radion-Higgs diphoton decay rate. For positive mixing parameter, the branching ratio of the light mixed radion (till 150 GeV) decaying to diphoton increases and hence can be probed with the diphoton channel at the LHC [19]. We shall explore this possibility in further studies.

In an earlier work some of us showed that the LHC data at 8 TeV can constrain the radion rather effectively, in a mass range upward of 110 GeV. And now we have found that the range below 110 GeV, all the way down to 60 GeV, is also accessible to probe at the LHC, for the integrated luminosity crossing the attobarn level.

ACKNOWLEDGMENTS

We thank Anushree Ghosh, Manoj K. Mandal and V. Ravindran for helpful comments. The work of U. M., B. M. and S. K. R. was partially supported by funding available from the Department of Atomic Energy, Government of India, for the Regional Centre for Accelerator-based Particle Physics (RECAPP), Harish-Chandra Research Institute. Computational work for this study was partially carried out at the cluster computing facility in the Harish Chandra Research Institute (http://cluster.hri.res.in). M. F. is supported in part by NSERC under Grant No. SAP105354 and would like to thank Manuel Toharia for illuminating discussions on radions. K. H. acknowledges support from the Academy of Finland (Project No. 137960). M. F., B. M. and S. K. R. thank the Helsinki Institute of Physics, while M. F. and K. H. thank RECAPP for hospitality at various stages of the project.

APPENDIX: DECAY RATES OF THE RADION

(i) *Tree-level decay rates for φ*

The decay widths of the radion to the SM particles are easily calculated from Eqs. (8), (10), (11) (see also [52]):

$$\Gamma(\varphi \to f\bar{f}) = \frac{N_c m_f^2 m_\varphi}{8\pi\Lambda_\varphi^2}(1-x_f)^{3/2}, \tag{A1}$$

$$\Gamma(\varphi \to W^+W^-) = \frac{m_\varphi^3}{16\pi\Lambda_\varphi^2}\sqrt{1-x_W}\left(1-x_W+\frac{3}{4}x_W^2\right), \tag{A2}$$

$$\Gamma(\varphi \to ZZ) = \frac{m_\varphi^3}{32\pi\Lambda_\phi^2}\sqrt{1-x_Z}\left(1-x_Z+\frac{3}{4}x_Z^2\right), \tag{A3}$$

$$\Gamma(\varphi \to hh) = \frac{m_\varphi^3}{32\pi\Lambda_\varphi^2}\sqrt{1-x_h}\left(1+\frac{1}{2}x_h\right)^2. \tag{A4}$$

The symbol f denotes all quarks and leptons. The variable x_i is defined as $x_i = 4m_i^2/m_\varphi^2 (i = t, f, W, Z, h)$.

(ii) *Loop-induced decay rates for $\varphi \to \gamma\gamma, gg$*

$$\Gamma(\varphi \to gg) = \frac{\alpha_s^2 m_\varphi^3}{32\pi^3\Lambda_\varphi^2}|b_3 + x_t\{1+(1-x_t)f(x_t)\}|^2, \tag{A5}$$

$$\Gamma(\varphi \to \gamma\gamma) = \frac{\alpha_{\mathrm{EM}}^2 m_\varphi^3}{256\pi^3\Lambda_\varphi^2}\Big|b_2 + b_Y - \{2+3x_W+3x_W(2-x_W)f(x_W)\} + \frac{8}{3}x_t\{1+(1-x_t)f(x_t)\}\Big|^2, \tag{A6}$$

$$\Gamma(\varphi \to Z\gamma) = \frac{\alpha_{\mathrm{EM}}^2 m_\varphi^3}{128\pi^3 s_{\mathrm{w}}^2\Lambda_\varphi^2}\left(1-\frac{m_Z^2}{m_\varphi^2}\right)^3 \times \Big|\sum_f N_f \frac{Q_f}{c_{\mathrm{W}}}\hat{v}_f A_{1/2}^\varphi(x_f,\lambda_f) + A_1^\varphi(x_W,\lambda_W)\Big|^2. \tag{A7}$$

Here, as before, $x_i = 4m_i^2/m_\varphi^2 (i = t, f, W, Z, h)$, and $\lambda_i = 4m_i^2/m_Z^2 (i = f, W)$. Here $(b_3, b_2, b_Y) = (7, 19/6, -41/6)$. The gauge couplings for QCD and QED are given by α_s and α_{EM}, respectively. The factor N_f is the number of active quark flavors in the 1-loop diagrams and N_c is 3 for quarks and 1 for leptons. Q_f and $\hat{v}_f$ denote the electric charge of the fermion and the reduced vector coupling in the $Zf\bar{f}$ interactions $\hat{v}_f = 2I_f^3 - 4Q_f s_W^2$, where I_f^3 denotes the weak isospin and $s_W^2 \equiv \sin^2\theta_W$, $c_W^2 = 1 - s_W^2$.

The form factors $A_{1/2}^{\varphi}(x,\lambda)$ and $A_1^{\varphi}(x,\lambda)$ are given by

$$A_{1/2}^{\varphi}(x,\lambda) = I_1(x,\lambda) - I_2(x,\lambda), A_1^{\varphi}(x,\lambda) = c_W\left\{4\left(3-\frac{s_W^2}{c_W^2}\right)I_2(x,\lambda) + \left[\left(1+\frac{2}{x}\right)\frac{s_W^2}{c_W^2} - \left(5+\frac{2}{x}\right)\right]I_1(x,\lambda)\right\}. \tag{A8}$$

The functions $I_1(x,\lambda)$ and $I_2(x,\lambda)$ are

$$I_1(x,\lambda) = \frac{x\lambda}{2(x-\lambda)} + \frac{x^2\lambda^2}{2(x-\lambda)^2}[f(x^{-1}) - f(\lambda^{-1})] + \frac{x^2\lambda}{(x-\lambda)^2}[g(x^{-1}) - g(\lambda^{-1})],$$
$$I_2(x,\lambda) = -\frac{x\lambda}{2(x-\lambda)}[f(x^{-1}) - f(\lambda^{-1})], \tag{A9}$$

where the loop functions $f(x)$ and $g(x)$ in (A5), (A6) and (A9) are given by

$$f(x) = \begin{cases} \left\{\sin^{-1}\left(\frac{1}{\sqrt{x}}\right)\right\}^2 & ,x \geq 1 \\ -\frac{1}{4}\left(\log\frac{1+\sqrt{1-x}}{1-\sqrt{1-x}} - i\pi\right)^2 & ,x < 1 \end{cases}, \tag{A10}$$

$$g(x) = \begin{cases} \sqrt{x^{-1}-1}\sin^{-1}\sqrt{x} & ,x \leq 1 \\ \frac{\sqrt{1-x^{-1}}}{2}\left(\log\frac{1+\sqrt{1-x^{-1}}}{1-\sqrt{1-x^{-1}}} - i\pi\right) & ,x > 1 \end{cases}. \tag{A11}$$

[1] G. Aad *et al.* (ATLAS Collaboration), Phys. Lett. B **716**, 1 (2012).
[2] S. Chatrchyan *et al.* (CMS Collaboration), Phys. Lett. B **716**, 30 (2012).
[3] L. Randall and R. Sundrum, Phys. Rev. Lett. **83**, 3370 (1999).
[4] G. Aad *et al.* (ATLAS Collaboration), Phys. Rev. D **90**, 052005 (2014).
[5] W. D. Goldberger and M. B. Wise, Phys. Rev. Lett. **83**, 4922 (1999).
[6] H. Davoudiasl, J. L. Hewett, and T. G. Rizzo, Phys. Rev. Lett. **84**, 2080 (2000).
[7] W. D. Goldberger and M. B. Wise, Phys. Lett. B **475**, 275 (2000).
[8] U. Mahanta and A. Datta, Phys. Lett. B **483**, 196 (2000).
[9] R. Barate *et al.*, (Phys. Lett. B **565**, 61 (2003).
[10] G. Aad *et al.* (ATLAS Collaboration), Phys. Rev. Lett. **113**, 171801 (2014).
[11] G. F. Giudice, R. Rattazzi, and J. D. Wells, Nucl. Phys. **B595**, 250 (2001).
[12] C. Csaki, M. L. Graesser, and G. D. Kribs, Phys. Rev. D **63**, 065002 (2001).
[13] C. Csaki, M. Graesser, L. Randall, and J. Terning, Phys. Rev. D **62**, 045015 (2000).
[14] D. Dominici, B. Grzadkowski, J. F. Gunion, and M. Toharia, Nucl. Phys. **B671**, 243 (2003).
[15] C. Csaki, J. Hubisz, and S. J. Lee, Phys. Rev. D **76**, 125015 (2007).
[16] J. F. Gunion, M. Toharia, and J. D. Wells, Phys. Lett. B **585**, 295 (2004).
[17] M. Chaichian, A. Datta, K. Huitu, and Z. h. Yu, Phys. Lett. B **524**, 161 (2002).
[18] T. G. Rizzo, arXiv:hep-ph/0207113.
[19] M. Toharia, Phys. Rev. D **79**, 015009 (2009).
[20] M. Battaglia, S. De Curtis, A. De Roeck, D. Dominici, and J. F. Gunion, Phys. Lett. B **568**, 92 (2003).
[21] N. Desai, U. Maitra, and B. Mukhopadhyaya, J. High Energy Phys. 10 (2013) 093.
[22] H. de Sandes and R. Rosenfeld, Phys. Rev. D **85**, 053003 (2012).
[23] H. Kubota and M. Nojiri, Phys. Rev. D **87**, 076011 (2013).
[24] D. W. Jung and P. Ko, Phys. Lett. B **732**, 364 (2014); B. Bellazzini, C. Csaki, J. Hubisz, J. Serra, and J. Terning, Eur. Phys. J. C **73**, 2333 (2013).
[25] M. Geller, S. Bar-Shalom, and A. Soni, Phys. Rev. D **89**, 095015 (2014).
[26] P. Cox, A. D. Medina, T. S. Ray, and A. Spray, J. High Energy Phys. 02 (2014) 032.
[27] H. Kubota and M. Nojiri, Phys. Rev. D **90**, 035006 (2014).
[28] Y. Ohno and G. C. Cho, EPJ Web Conf. **49**, 18003 (2013).
[29] V. P. Goncalves and W. K. Sauter, Phys. Rev. D **82**, 056009 (2010).

[30] V. Barger, M. Ishida, and W. Y. Keung, Phys. Rev. Lett. **108**, 101802 (2012).

[31] K. Cheung and T. C. Yuan, Phys. Rev. Lett. **108**, 141602 (2012).

[32] H. Davoudiasl, T. McElmurry, and A. Soni, Phys. Rev. D **86**, 075026 (2012).

[33] Z. Chacko and R. K. Mishra, Phys. Rev. D, **87**, 115006 (2013); Z. Chacko, R. K. Mishra, and D. Stolarski, J. High Energy Phys. 09 (2013) 121.

[34] Z. Chacko, R. Franceschini, and R. K. Mishra, J. High Energy Phys. 04 (2013) 015.

[35] G. C. Cho, D. Nomura, and Y. Ohno, Mod. Phys. Lett. A **28**, 1350148 (2013).

[36] M. Pieri *et al.*, Report No. CMS-NOTE-2006-112.

[37] B. Grzadkowski, J. F. Gunion, and M. Toharia, Phys. Lett. B **712**, 70 (2012).

[38] CMS Collaboration, Report No. CMS-PAS-HIG-13-011.

[39] H. Davoudiasl, T. McElmurry, and A. Soni, Phys. Rev. D **82**, 115028 (2010); **86**, 039907(E) (2012).

[40] T. Binoth, J. P. Guillet, E. Pilon, and M. Werlen, Eur. Phys. J. C **16**, 311 (2000).

[41] B. Gombar (private communication).

[42] T. Stelzer and W. F. Long, Comput. Phys. Commun. **81**, 357 (1994); F. Maltoni and T. Stelzer, J. High Energy Phys. 02 (2003) 027; J. Alwall, M. Herquet, F. Maltoni, O. Mattelaer, and T. Stelzer, J. High Energy Phys. 06 (2011) 128.

[43] N. D. Christensen and C. Duhr, Comput. Phys. Commun. **180**, 1614 (2009); N. D. Christensen, P. de Aquino, C. Degrande, C. Duhr, B. Fuks, M. Herquet, F. Maltoni, and S. Schumann, Eur. Phys. J. C **71**, 1541 (2011).

[44] T. Sjostrand, S. Mrenna, and P. Z. Skands, J. High Energy Phys. 05 (2006) 026; Comput. Phys. Commun. **178**, 852 (2008).

[45] J. Pumplin, D. R. Stump, J. Huston, H. L. Lai, P. M. Nadolsky, and W. K. Tung, J. High Energy Phys. 07 (2002) 012.

[46] CMS Collaboration, Report No. CMS-PAS-EGM-10-003.

[47] M. Cacciari, G. P. Salam, and G. Soyez, J. High Energy Phys. 04 (2008) 063.

[48] V. Ravindran (private communication).

[49] Z. Bern, L. Dixon, and C. Schmidt, arXiv:hep-ph/0211216; , Phys. Lett. B **738**, 274 (2014).

[50] G. Cowan, K. Cranmer, E. Gross, and O. Vitells, Eur. Phys. J. C **71**, 1554 (2011); **73**, 2501(E) (2013).

[51] S. Bhattacharya, S. S. Chauhan, B. C. Choudhary, and D. Choudhury, Phys. Rev. D **76**, 115017 (2007).

[52] K. M. Cheung, Phys. Rev. D **63**, 056007 (2001).